Electronic Supplementary Information

Examining the Substituent Effect on Mycosporine-inspired Ultraviolet Filters

Abigail L. Whittock,[1,2] Adam M. Cowden,[1,3] Martin Wills[1] and Vasilios G. Stavros[1,*]

[1]Department of Chemistry, University of Warwick, Coventry, CV4 7AL, United Kingdom
[2]Analytical Science Centre for Doctoral Training, Senate House, University of Warwick, Coventry, CV4 7AL, United Kingdom
[3]Molecular Analytical Science Centre for Doctoral Training, Senate House, University of Warwick, Coventry, CV4 7AL, United Kingdom

*Corresponding author: v.stavros@warwick.ac.uk

Experimental details and characterisation

General information

Melting points were obtained in open capillary tubes using micro melting point apparatus which were uncorrected. Mass spectra were recorded on a time of flight (TOF) mass spectrometer by the electrospray ionisation (ESI) method. ^{1}H nuclear magnetic resonance (NMR) spectra were recorded using $CDCl_3$ (δ_H = 7.26 ppm) or CD_3OD (δ_H = 4.87 ppm) as the solvent at ambient temperature on the 300 or 400 MHz spectrometer. Data are presented as follows: chemical shift (in ppm), integration, multiplicity (s = singlet, d = doublet, t = triplet and m = multiplet), coupling constant (J/Hz) and interpretation. ^{13}C NMR spectra were recorded by broadband spin decoupling for $CDCl_3$ (δ_C = 77.2 ppm) at ambient temperature and at 101 MHz. Chemical shift values are reported in ppm. Thin-layer chromatogram (TLC) was performed using commercially prepared 100–400 mesh silica gel plates, and visualisation was effected at 254 or 365 nm. Unless otherwise noted, all reagents and solvents were used as purchased. In cases where the compound has been made previously a reference is provided for full characterisation data.

Synthesis procedures

3-(Phenylamino)cyclohex-2-en-1-one (1).[1] 1,3-Cyclohexanedione (500 mg, 4.45 mmol) was added to 20% (v/v) acetic acid in water with stirring. Aniline (414 mg, 0.40 mL, 4.5 mmol) was added at room temperature and the mixture was stirred. The solution was then heated to reflux for 5 hours and stirred overnight. After cooling to room temperature, a solid was formed by adding small amounts of chilled distilled water to the solution. Once a precipitate had formed the product was isolated by filtration and dried under vacuum. The product was purified by washing several times with minimal amounts of ice cold ethyl acetate or by chromatography on a silica-gel column using a 1:99 to 10:90 methanol:DCM gradient. A yellow solid (365 mg, 1.95 mmol, 44%), R_f = 0.15 (ethyl acetate). Mp: 174-175 °C. ^{1}H NMR (400 MHz, $CDCl_3$) δ 7.34-7.29 (2H, m, ArH), 7.26-7.15 (3H, m, ArH), 6.56 (1H, brs, NH), 5.57 (1H, s, =CH), 2.50 (2H, t, *J*= 6.0 Hz, CH_2), 2.35 (2H, t, *J*= 6.0 Hz, CH_2), 2.04-2.00 (2H, m, CH_2) ppm. ^{13}C NMR (101 MHz, $CDCl_3$) 129.4 (ArC), 125.6 (ArC), 124.0 (ArC), 100.3 (=CH), 36.5 (CH_2), 29.2 (CH_2), 21.9 (CH_2) ppm (C=O and C ipsos do not show clearly). HRMS (ESI-TOF) calcd for $C_{12}H_{14}NO^+$ $[M+H]^+$ 188.1070, found: 188.1075.

2-Methyl-3-(phenylamino)cyclohex-2-enone (2).[2] 2-Methyl-1,3-cyclohexanedione (400 mg, 3.17 mmol) and aniline hydrochloride (450 mg, 3.47 mmol) were added to an oven-dried round bottom flask with a stirrer bar. Toluene (20 mL) was added, and the solution was heated to 120 °C for 2 days. After cooling to room temperature, the solution was transferred to a separating funnel, and equal volumes of ethyl acetate (10 mL) and saturated NH_4Cl solution (10 mL) were added. The organic layer was separated and washed with half volume of NH_4Cl solution and brine consecutively. The organic layer was concentrated under reduced pressure. Small portions of cool ethyl acetate were used to wash the concentrated residue until a pinkish-grey solid was formed, which was then dried and recrystallised from diethyl ether to give the product. An off-white solid (186 mg, 0.925 mmol, 29%), R_f = 0.15 (ethyl acetate). Mp: 140-142 °C. ^{1}H NMR (400 MHz, $CDCl_3$) δ 7.36 (2H, t, *J* = 7.8 Hz, ArH), 7.20 (1H, t, *J* = 7.4 Hz, ArH), 7.08 (2H, d, *J* = 7.8 Hz, ArH), 6.23 (1H, brs, NH), 2.48-2.45 (2H, m, CH_2), 2.41-2.38 (2H, m, CH_2), 1.94-1.90 (2H, m, CH_2) ppm, 1.86 (3H, s, CH_3). ^{13}C NMR (101 MHz, $CDCl_3$) 129.3 (ArC), 125.5 (ArC), 124.8 (ArC), 77.0, 36.2 (CH_2), 27.0 (CH_2), 22.0 (CH_2), 8.1 (CH_3) ppm. (C=O and C ipsos do not show clearly). HRMS (ESI-TOF) calcd for $C_{13}H_{16}NO^+$ $[M+H]^+$ 202.1226, found: 202.1228.

2-Methoxy-3-(phenylamino)cyclohex-2-enone (3). 3-Hydroxy-2-methoxycyclohex-2-enone (100 mg, 0.70 mmol) was added, with aniline hydrochloride (130 mg, 1.0 mmol), to a round bottom flask. Toluene (5 mL), and molecular sieves were added, the solution was heated to reflux for 5 hours and then stirred overnight with no heating. At room temperature, the solvent was decanted off and a 1:1 (v/v) mixture of ethyl acetate and saturated NH_4Cl solution (10 mL total) was added to the remaining residue. The mixture was filtered into a separating funnel. The organic layer was separated, and the remaining aqueous solution was extracted further with ethyl acetate (2 x 10 mL). The organic layers were combined, dried over sodium sulphate, and concentrated under reduced pressure to yield the product. A white solid (101 mg, 0.47 mmol, 66%). ^{1}H NMR (400 MHz, $CDCl_3$) δ 7.36 (2H, t, *J* = 7.5 Hz, ArH), 7.28 (1H, brs, NH), 7.19 (1H, t, *J* = 7.5 Hz, ArH), 7.09 (2H, d, *J*= 7.8 Hz, ArH), 3.78 (3H, s, OCH_3), 2.57 (2H, t, *J* = 6.0 Hz, CH_2), 2.44 (2H, t, *J* = 6.0 Hz, CH_2), 1.95-1.89 (2H, m, CH_2) ppm. ^{13}C NMR (101 MHz, $CDCl_3$) 189.4 (C=O), 152.0 (C), 138.2 (C), 133.2 (C), 129.3 (ArCH), 125.2 (ArCH), 124.0 (ArCH), 59.6 (CH), 37.0 (CH_2), 26.0 (CH_2), 21.8 (CH_2) ppm. HRMS (ESI-TOF) calcd for $C_{13}H_{16}NO_2$+ $[M+H]^+$ 218.1176, found: 218.1179.

2-Hydroxy-3-(phenylamino)cyclohex-2-enone (4).[3] 2,3-Dihydroxycyclohex-2-en-1-one (400 mg, 3.13 mmol), and freshly prepared aniline hydrochloride (420 mg, 3.24 mmol) were mixed well in a round bottom flask. Minimum distilled water (~2 mL) was added with stirring until all had dissolved and the solution was then stirred at room temperature while being purged with nitrogen for 30 minutes, or until a solid formed. The flask was then sealed and transferred to the fridge overnight. The solid product thus formed was filtered, washed with minimal cold toluene, and dried under vacuum and not purified further. An off-white solid (112 mg, 0.55 mmol, 18%). Mp: 120-122 °C. ^{1}H NMR (400 MHz, $CDCl_3$) δ 7.36-7.32 (2H, m, ArH), 7.17-7.14 (1H, m, ArH), 7.08-7.06 (2H, m, ArH), 6.80 (1H, broad, NH), 5.65 (1H, s, =CH), 2.64-2.61 (2H, m, CH_2), 2.49-2.47 (2H, m, CH_2), 2.00-1.95 (2H, m, CH_2) ppm. ^{13}C NMR (101 MHz, $CDCl_3$) 188.3 (C=O), 142.3 (C), 138.6 (C), 129.7 (C), 129.3 (ArCH), 124.7 (ArCH), 123.3 (ArCH), 34.4 (CH_2), 25.4 (CH2), 21.8 (CH_2). HRMS (ESI-TOF) calcd for $C_{12}H_{14}NO_2$+ $[M+H]^+$ 204.1019, found: 204.1016.

2,3-Dihydroxycyclohex-2-en-1-one (Dihydropyrogallol).[4] Pyrogallol (Benzene-1,2,3-triol) (6.3 g, 50 mmol) was added to a basic solution (2.0 g NaOH in 12.6 mL H_2O) in the glass insert of a Parr high pressure reactor with a stirrer bar at room temperature. Raney Nickel (~2.1 g, ~12.8 mmol) was added and the reactor was pressurised to 69 bar H_2 and the temperature was increased to 60 °C for 5 hours with stirring. Then the reactor was allowed to cool to room temperature overnight before depressurising. The mixture was then filtered, and the filtrate was cooled in an ice bath (<5 °C) and acidified dropwise with 37% HCl. On standing for 30 minutes a greyish precipitate formed and was filtered. On further acidification an off-white product (2.7 g, 21.1 mol, 42%) was obtained. The precipitate was filtered and redissolved in minimal hot ethyl acetate and dried in vacuo. A further portion of product mixed with starting material as a brown oil can be recovered by extracting the mother liquor with ethyl acetate (3 x 10 cm^3), drying the combined organic layers with anhydrous sodium sulphate, and drying under vacuum. Note: if the reaction is incomplete then the product may not crystallise, and the starting material/product mixture can be isolated through extraction with ethyl acetate in

this case. The aqueous solution should not be diluted as this will reduce the yield due to the water solubility of the reagent and product. Too long a reaction time will result in over-reduction. The product was isolated as an off-white solid (2.7 g, 21.1 mmol, 42%), R_f = 0.2-0.3 (ethyl acetate-hexane 1:1). ^{1}H NMR (400 MHz, CD_3OD) δ 2.43 (4H, t, *J* = 6.4 Hz, $C\underline{H}_2CH_2C\underline{H}_2$), 1.98-1.92 (2H, m, $CH_2C\underline{H}_2CH_2$) ppm. LRMS m/z: [M+Na]+ 151.0.

3-Hydroxy-2-methoxycyclohex-2-en-1-one.[3] 2,3-Dihydroxycyclohex-2-en-1-one (2.40 g, 18.8 mmol) was dissolved in aqueous NaOH (4M, 10 mL, 40 mmol) and stirred under nitrogen in an iced water bath (<5 °C) for 10 minutes. Dimethyl sulphate (5.0 g, 3.8 mL, 40.1 mmol, 2.1 eq.) was added by dropping funnel over 10 minutes and the mixture was stirred for 30 minutes. Then a second portion of NaOH (4M, 10 mL, 40 mmol) was added by syringe and the flask was removed from the bath and gradually allowed to warm to room temperature over 18 hours with stirring. The resulting solution was cooled to room temperature by placing in an iced water bath and acidified to pH ~4-5 dropwise with concentrated HCl (~2 mL) and extracted with diethyl ether (3 x 25 mL) with vigorous stirring. The combined ether extracts were dried over anhydrous sodium sulphate and the solvent was removed in vacuo to leave the product. A pale yellow solid (560 mg, 3.94 mmol, 21%), R_f = 0.8 (ethyl acetate-methanol 9:1). ^{1}H NMR (300 MHz, $CDCl_3$) 6.20 (1H, brs, OH), 3.73 (3H, s, OCH_3), 2.49-2.45 (4H, m, $CH_2CH_2CH_2$), 1.97-1.93 (2H, m, $CH_2CH_2CH_2$) ppm. LRMS m/z: [M+H]+ Found 143.1.

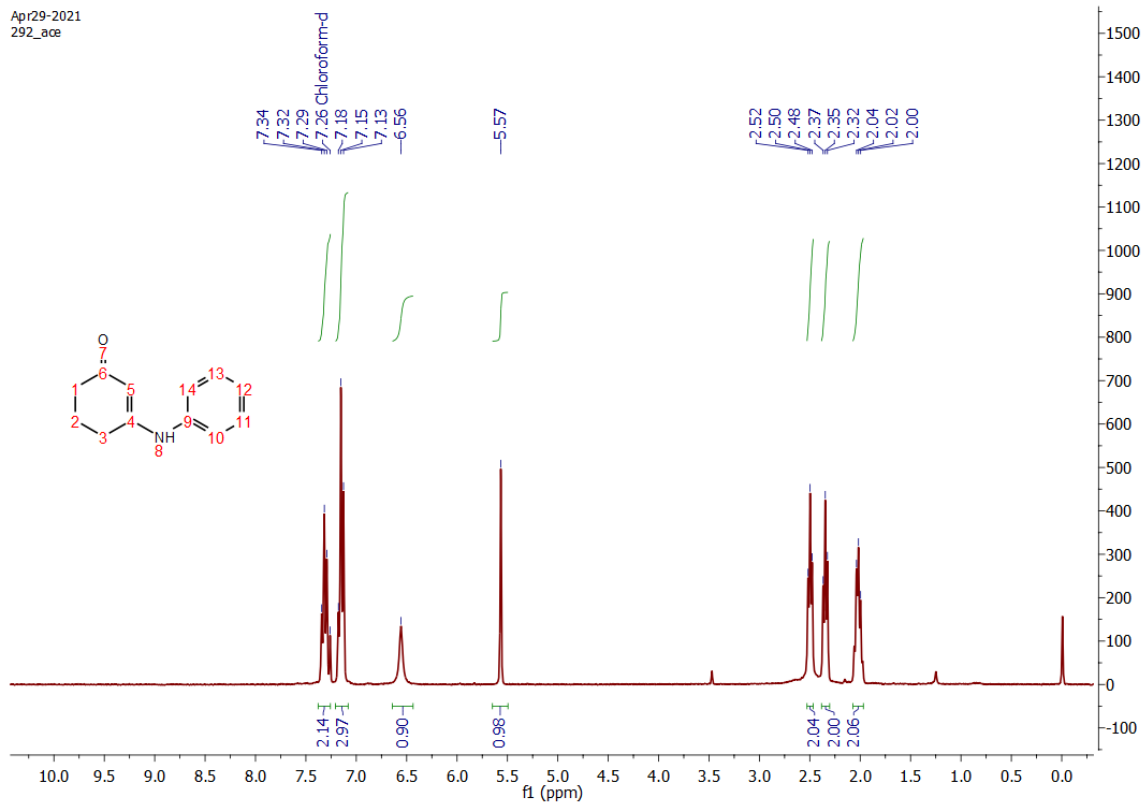

Figure S1. ^{1}H NMR spectrum (400 MHz) of **1** in $CDCl_3$.

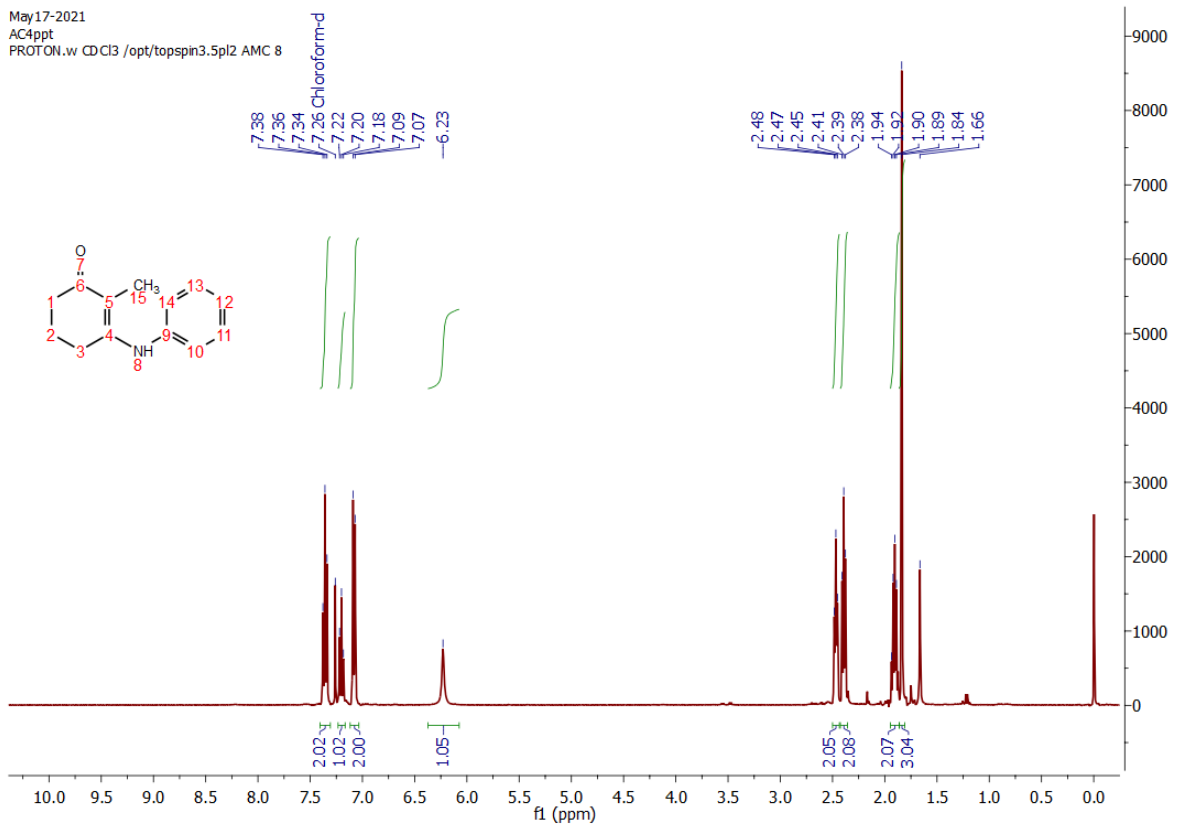

Figure S2. ^{1}H NMR spectrum (400 MHz) of **2** in $CDCl_3$.

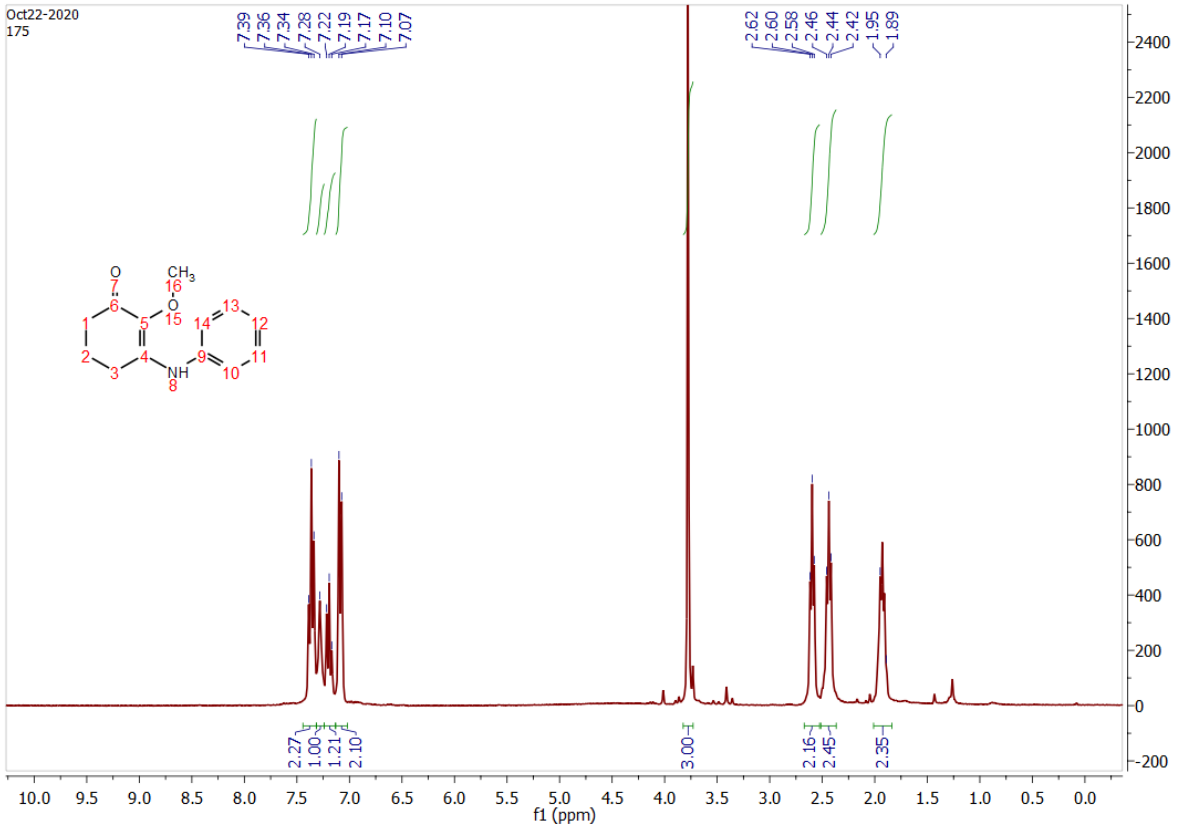

Figure S3. ^{1}H NMR spectrum (400 MHz) of **3** in $CDCl_3$.

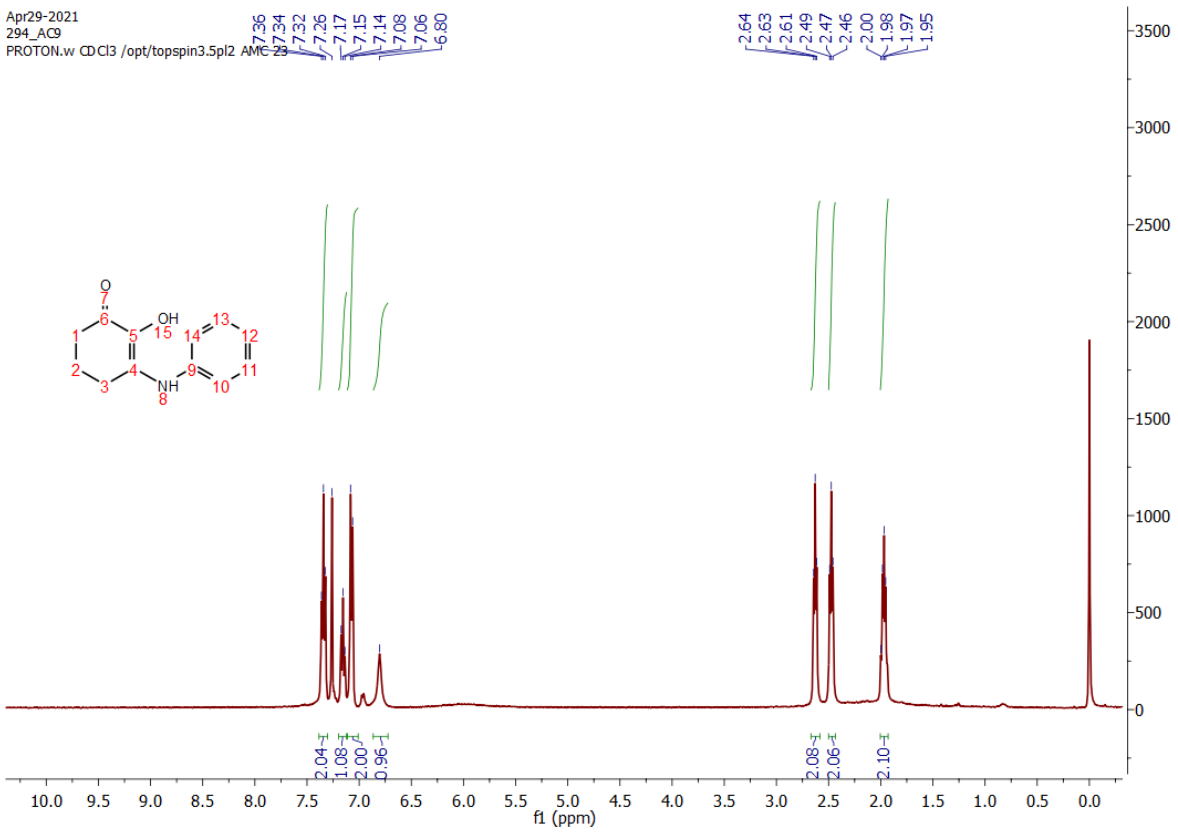

Figure S4. ^{1}H NMR spectrum (400 MHz) of **4** in $CDCl_3$.

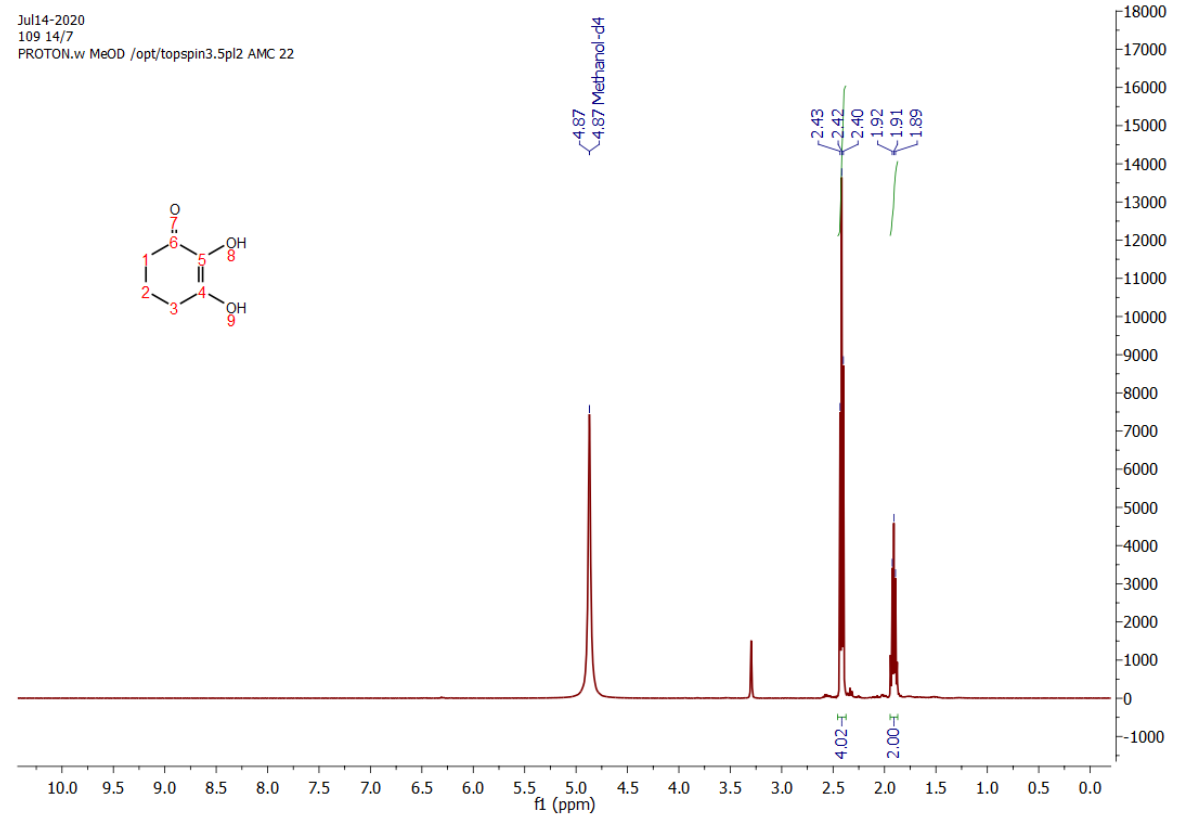

Figure S5. ^{1}H NMR spectrum (400 MHz) of 2,3-Dihydroxycyclohex-2-en-1-one in CD_3OD.

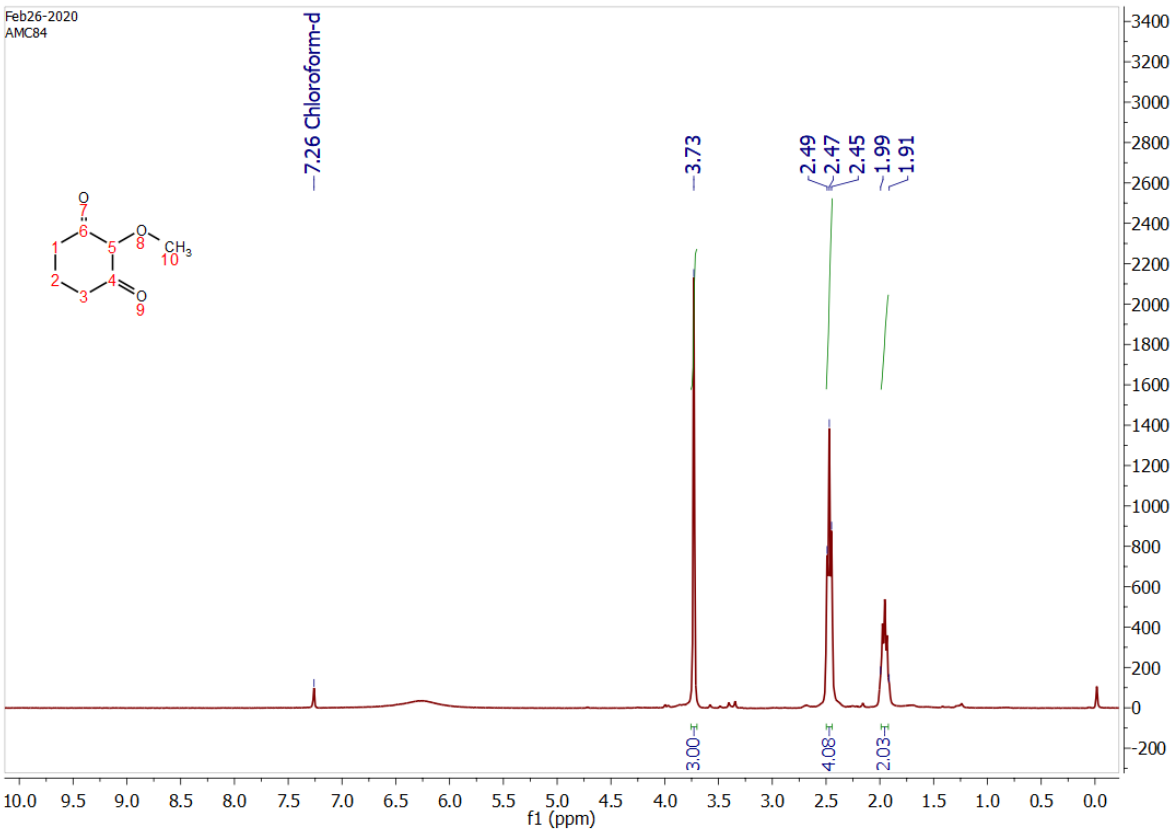

Figure S6. ^{1}H NMR spectrum (300 MHz) of 3-Hydroxy-2-methoxycyclohex-2-en-1-one in $CDCl_3$.

Electronic ground state geometry optimisation discussion

Within the main manuscript, we discussed the relaxed geometries of **1**-**4** computed at the DFT/PBE0/6-311++G** level in implicitly modelled water. Here we describe the geometries again but with some additional details. For all optimisations, we observed that the phenyl ring was twisted out of the plane to the cyclohexenone ring by ~50° likely due to steric effects. Two conformers were considered around the C-3–N bond; **a** when the C–C–N–C dihedral angle, highlighted in pink in **Figure S7**a, is around 0° and **b** when the C–C–N–C dihedral angle is around 180°. The relative energies of each conformer, their computed structure and the C–C–N–C angle is presented in **Figure S7**b. The lower energy conformer was **a** for **1** and **b** for **2**-**4**. In all cases, the energy difference between the conformers is ≤0.1 eV, suggesting that the lower energy conformer dominates in aqueous solution (less so for **2** and **4** given a smaller energy gap between the conformers of 0.03 and 0.02 eV, respectively). We suggest that **b** being the lower energy conformer for **2**-**4** may be due to several reasons; steric effects experienced by the bulkier substituents at C-2, solvent interaction or another intramolecular interaction. This steric hinderance is also reflected in the C–C–N–C dihedral angle for conformer **a** in **2**-**4** which is twisted 19-34° out of plane. The final geometry-related note is that for **3**, the methoxy group is perpendicular to the plane of the molecule similar to that of natural mycosporine-like amino acids,[5] whereas for **4**, the hydroxy group is in the plane of the molecule and forms an intramolecular hydrogen bond with the ketone at C-1.

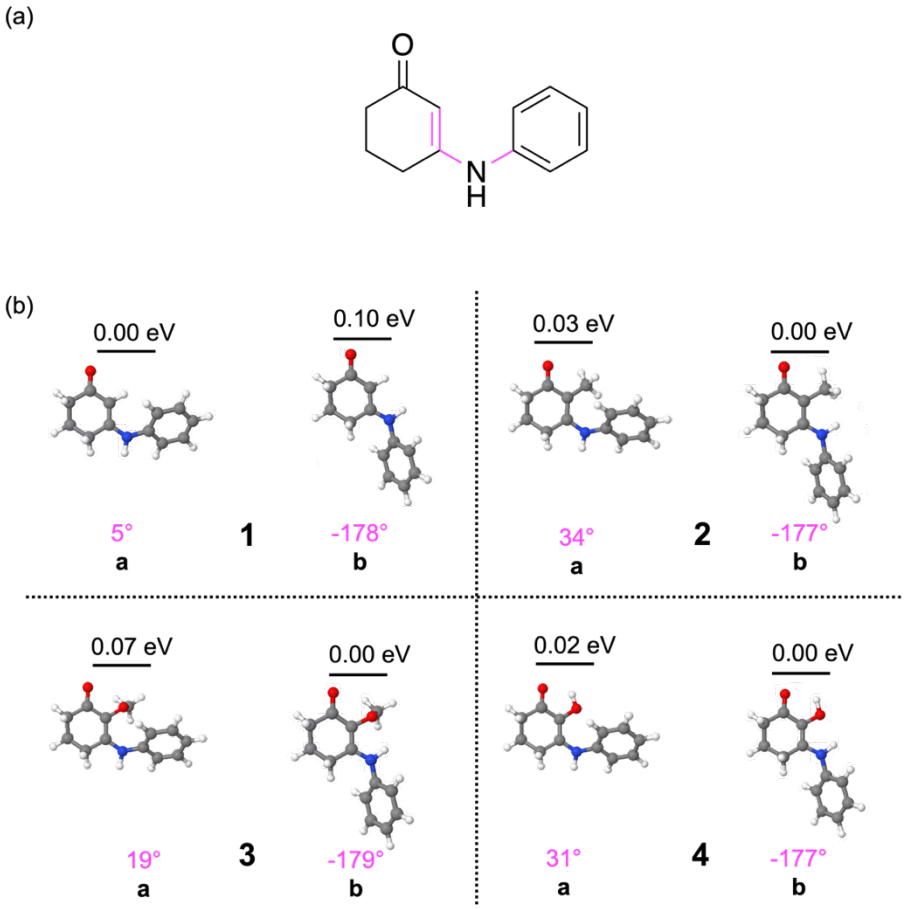

Figure S7. (a) Structure of **1** with the C–C–N–C dihedral angle highlighted in pink. (b) Schematic representation of the relative energies of the conformers of **1**-**4** with respect to their lowest energy conformer along with their optimised geometries and the C–C–N–C dihedral angles of each conformer reported in pink. Note that (b) is not drawn to scale.

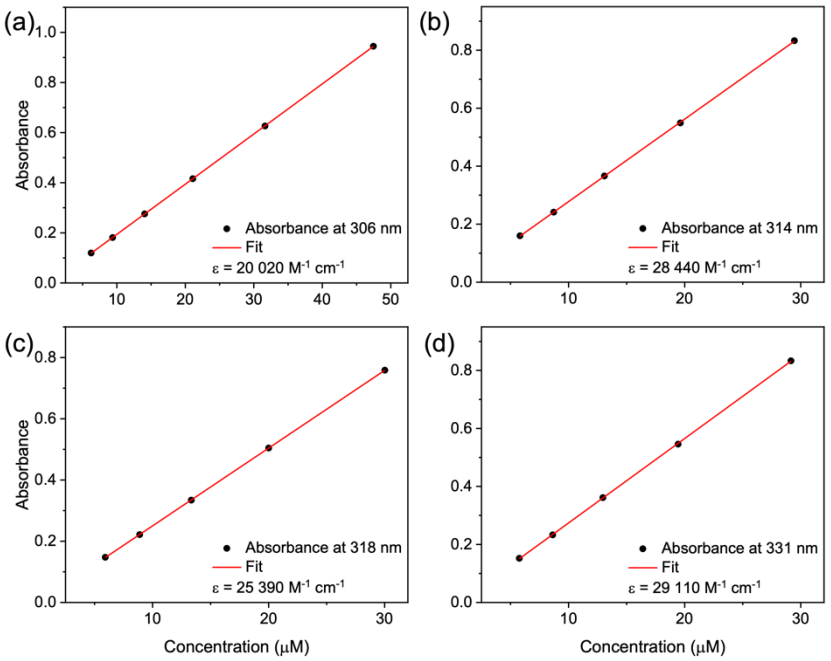

Figure S8. Concentration vs absorbance plots for (a) **1**, (b) **2**, (c) **3** and (d) **4** in water. The filled black circles are the raw data and the red lines are the linear fit where the gradient is equivalent to the molar extinction coefficient.

Singlet vertical excitation energies

Table S1. Calculated singlet vertical excitation energies for the optimised S_0 geometries of **1**-**4** in implicitly modelled water at the RI-CC2/def2-TZVP level.

Molecule (conformer)	State	Energy (eV)	Energy (nm)	Oscillator strength	Character
1 (a)	S_1	4.17	297	0.0937	nπ*
	S_2	4.29	289	0.6040	ππ*
	S_3	4.86	255	0.0172	ππ*
	S_4	5.76	215	0.1351	ππ*
	S_5	5.99	207	0.1294	ππ*
1 (b)	S_1	4.17	297	0.0591	nπ*
	S_2	4.32	287	0.9522	ππ*
	S_3	4.94	251	0.0084	ππ*
	S_4	5.69	218	0.0025	ππ*
	S_5	5.99	207	0.0927	ππ*
2 (a)	S_1	4.05	306	0.2276	nπ*
	S_2	4.19	296	0.4442	ππ*
	S_3	4.74	262	0.0218	ππ*
	S_4	5.63	220	0.1024	ππ*
	S_5	5.92	209	0.1120	ππ*
2 (b)	S_1	4.14	300	0.1019	nπ*
	S_2	4.30	288	0.8498	ππ*
	S_3	4.91	252	0.0088	ππ*
	S_4	5.56	223	0.0051	ππ*
	S_5	5.86	212	0.0537	ππ*
3 (a)	S_1	4.12	301	0.3123	nπ*
	S_2	4.19	296	0.4052	ππ*
	S_3	4.84	256	0.0075	ππ*
	S_4	5.47	227	0.0497	nπ*
	S_5	5.68	218	0.0856	ππ*
3 (b)	S_1	4.15	299	0.3568	nπ*
	S_2	4.20	295	0.5864	ππ*
	S_3	4.90	253	0.0098	ππ*
	S_4	5.54	224	0.0071	ππ*
	S_5	5.84	212	0.0559	ππ*
4 (a)	S_1	3.81	325	0.6360	ππ*
	S_2	4.40	282	0.0029	nπ*
	S_3	4.73	262	0.0167	ππ*
	S_4	5.47	227	0.1649	ππ*
	S_5	5.62	221	0.0687	ππ*
4 (b)	S_1	3.87	321	0.8810	ππ*
	S_2	4.39	282	0.0056	nπ*
	S_3	4.79	259	0.0145	ππ*
	S_4	5.38	230	0.0280	ππ*
	S_5	5.77	215	0.0439	ππ*

Table S2. Orbitals involved in the S_1 and S_2 transitions for the lowest energy conformer of **1**-**4**.

Molecule (conformer)	$S_0 \rightarrow S_1$	$S_0 \rightarrow S_2$
1 (a)	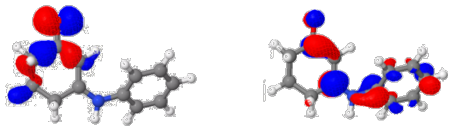	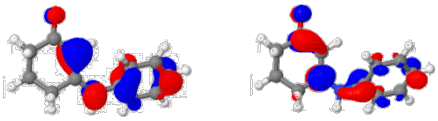
2 (b)	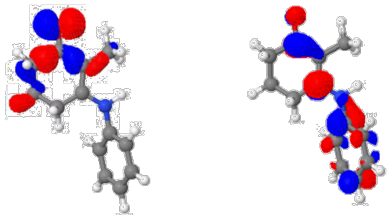	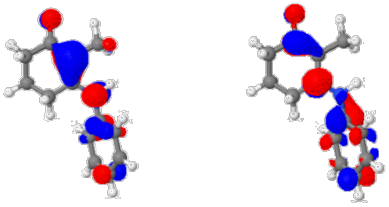
3 (b)	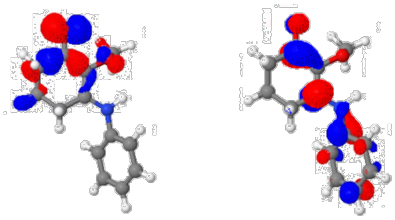	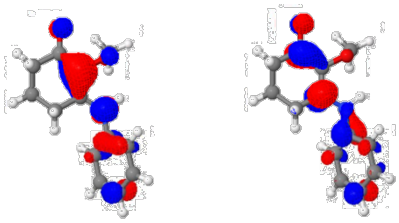
4 (b)	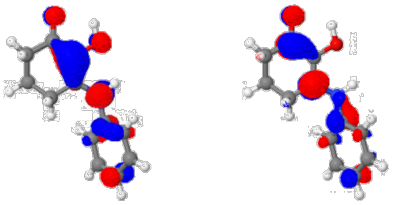	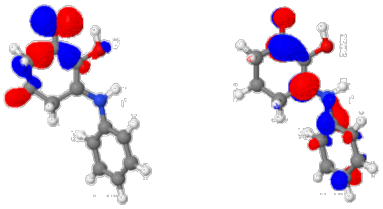

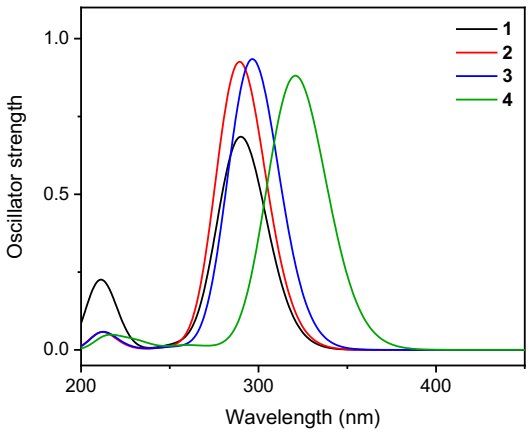

Figure S9. Predicted UV-visible spectra of **1**-**4** (lowest energy conformer) plotted as a sum of Gaussians of the first five singlet vertical excitation energies with a fixed width of 0.2 eV for each Gaussian.

TAS presented in several ways

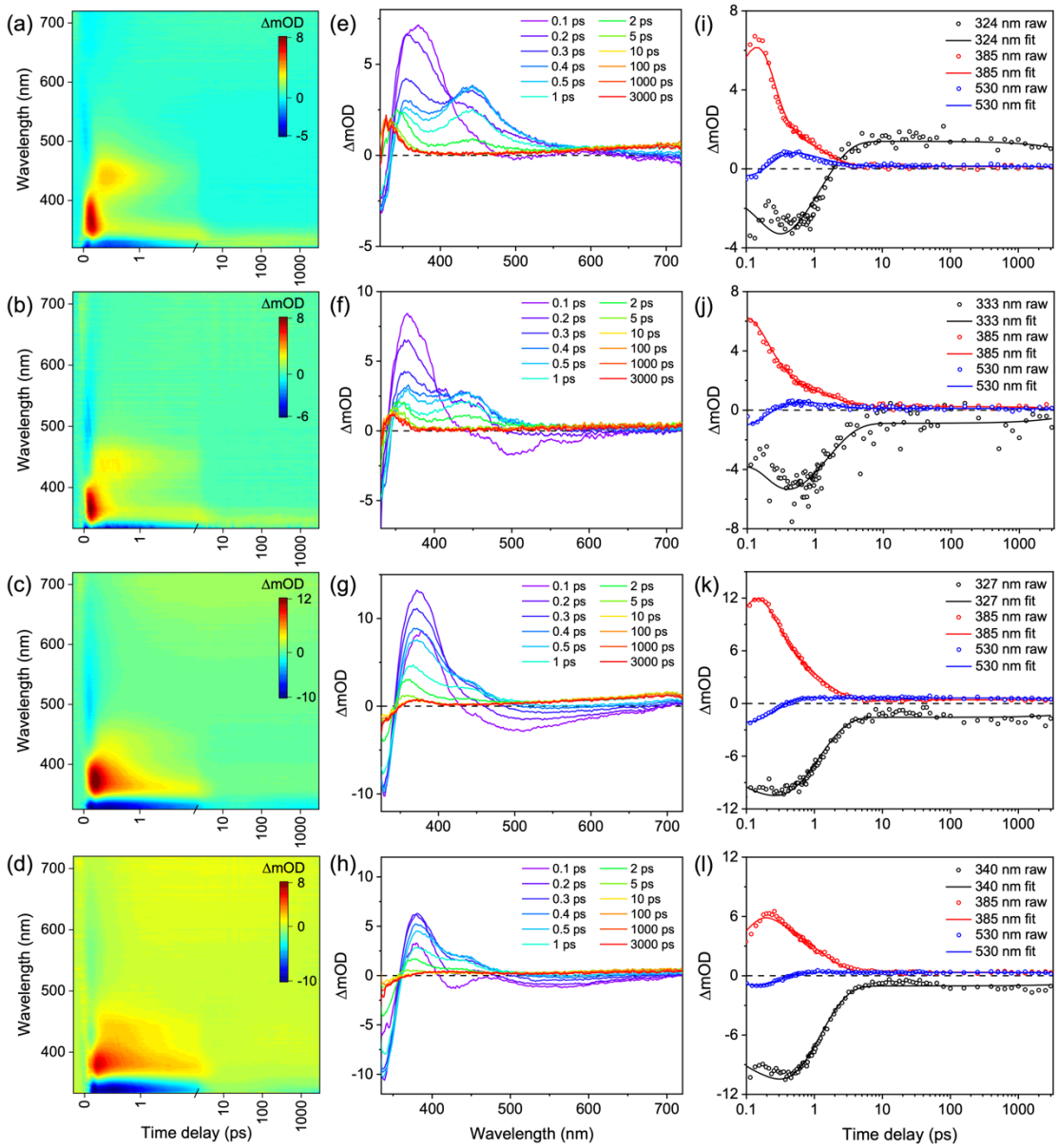

Figure S10. TAS displayed as (a-d) false colour heat maps and (e-h) lineouts at selected pump-probe time delays for aqueous solutions of (a, e) **1** photoexcited at 306 nm, (b, f) **2** photoexcited at 314 nm, (c, g) **3** photoexcited at 318 nm and (d, h) **4** photoexcited at 331 nm. In (a-d) time delay is plotted linearly until 2 ps and then as a logarithmic scale between 2 and 3000 ps. Transients at selected wavelengths for aqueous solutions of (i) **1** photoexcited at 306 nm, (j) **2** photoexcited at 314 nm, (k) **3** photoexcited at 318 nm and (l) **4** photoexcited at 331 nm. The open circles are the raw data and the solid lines are the fits.

TAS at 1 ns in potassium nitrate (KNO_3)

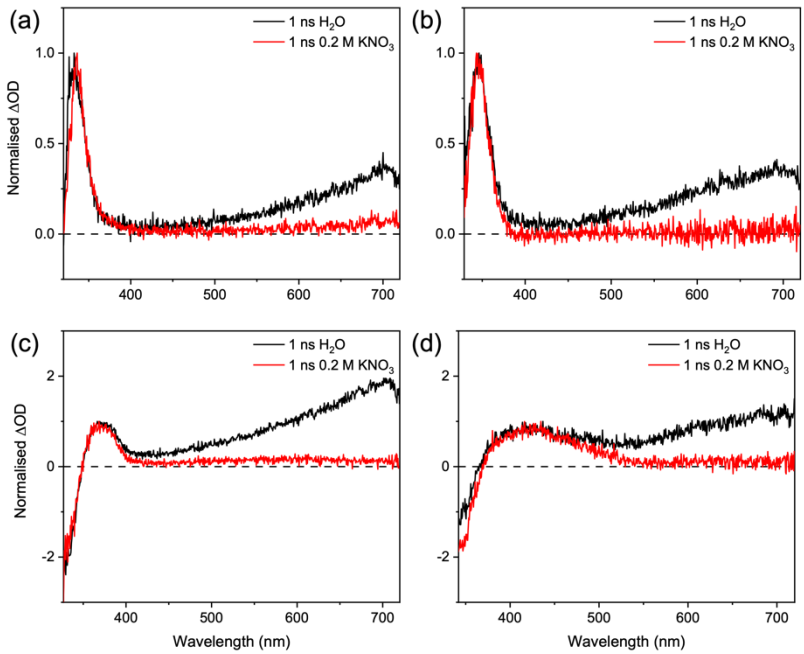

Figure S11. 1 ns TAS of (a) **1**, (b) **2** and (c) **3** and (d) **4** in aqueous solution (black trace) and in 0.2 M KNO_3 (red trace).

TAS of water

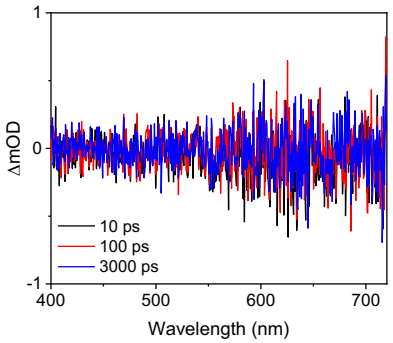

Figure S12. TAS taken at 100, 1000 and 3000 ps for water photoexcited at 314 nm from the solvent-only scan.

Power dependency

The power dependence of the excited state absorption feature ~340 nm and the solvated electron absorption feature ~660 nm was determined for **2**. This was achieved by varying the output power of the TOPAS-prime to several powers around the power used for the transient scans. 10 nm integration windows were selected (340-350 nm and 660-670 nm) at a specified Δt (100 ps). The gradient of the log(Signal) *vs.* log(Power) plot was around 1 and 2 respectively for each integration window, as can be seen in **Figure S13**, indicating that the solvated electron dynamics we have observed within this work is the result of multiphoton induced dynamics. The below data is only for **2** as an example but the other stable molecules show the same dependence. Note that multiphoton processes are unlikely to occur in nature and only occur in our TAS given that the photon density of our pulsed laser is much greater than a continuous light source (e.g., solar irradiance). As a result, we did not explore the solvated electron results within this work in detail.

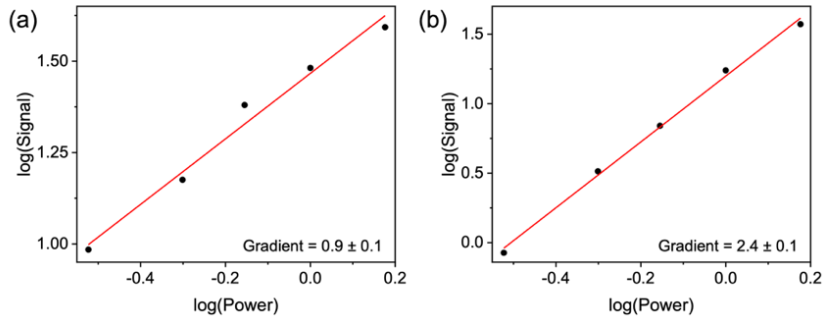

Figure S13. Power dependency of an aqueous solution of **2** photoexcited at 314 nm for (a) the excited state absorption at a Δt of 100 ps and an integration window between 340 and 350 nm and (b) the solvated electron at a Δt of 100 ps and an integration window between 660 and 670 nm. The power used for the TAS presented in the main manuscript was 500 μW which corresponds to -0.3 on the x axis.

Evolution associated difference spectra

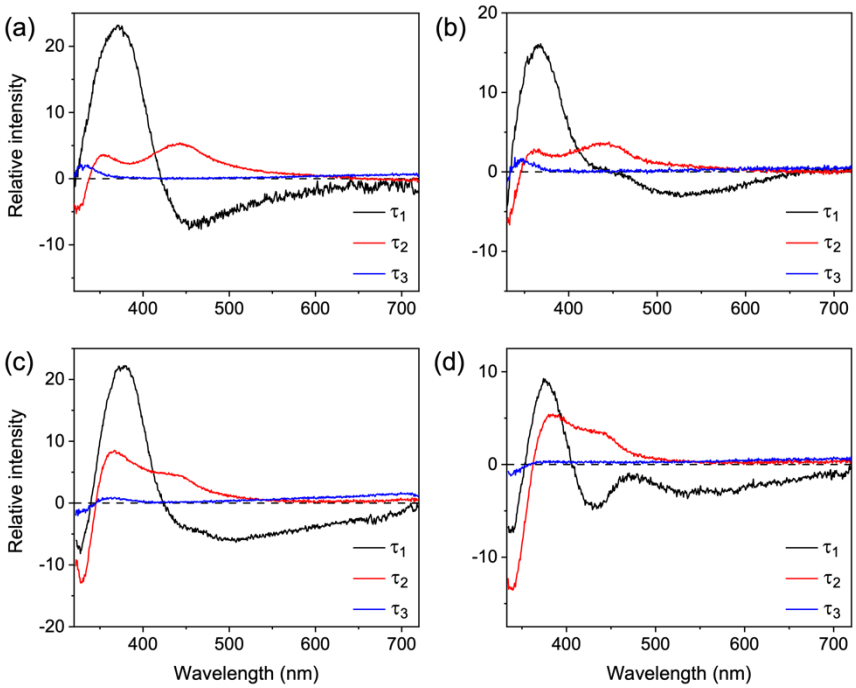

Figure S14. Evolution associated difference spectra for aqueous solutions of (a) **1** photoexcited at 306 nm, (b) **2** photoexcited at 314 nm, (c) **3** photoexcited at 318 nm and (d) **4** photoexcited at 331 nm.

Residuals

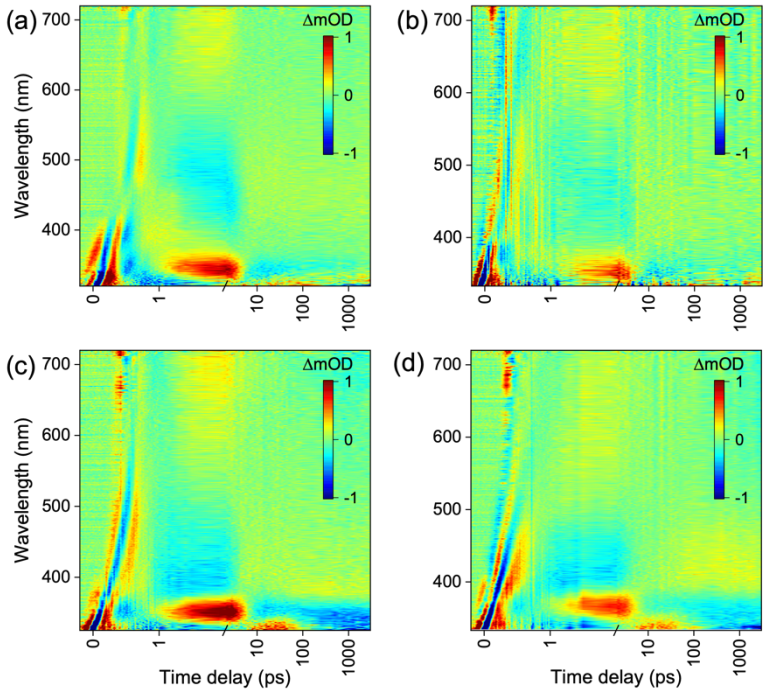

Figure S15. False colour heat maps of the fitting residual for aqueous solutions of (a) **1** photoexcited at 306 nm, (b) **2** photoexcited at 314 nm, (c) **3** photoexcited at 318 nm and (d) **4** photoexcited at 331 nm. Time delay is plotted linearly until 2 ps and then as a logarithmic scale from 2 to 3000 ps. The fitting residuals have not been chirp corrected.

Instrument response

We conducted solvent-only transients of water following photoexcitation at 314 nm to obtain the instrument response function which determines the limiting temporal resolution of our TAS. The value of the temporal resolution was acquired by fitting a Gaussian over the time-zero response of solvent-only scans and taking the full width half maximum (FWHM). All the quoted errors in **Table 2** of the main manuscript are half of the FWHM of the instrument response function rounded to the nearest 10 fs.

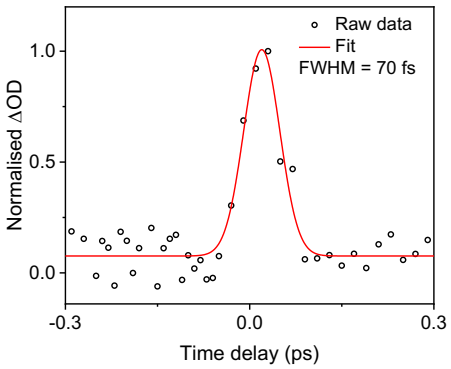

Figure S16. Averaged transient (388-390 nm) for solvent-only time-zero response of water photoexcited at 314 nm (black circles) with a Gaussian fit overlaid (red line); the returned FWHM is ~70 fs and corresponds to the FWHM of the instrument response function.

TAS of 1 in ethanol

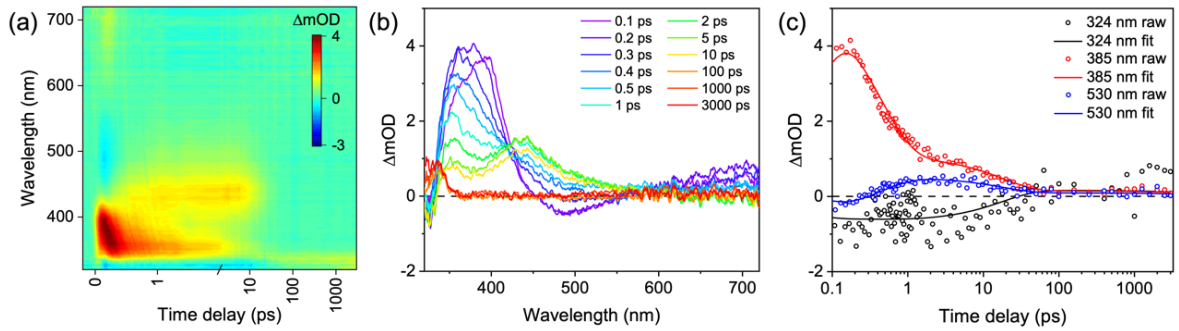

Figure S17. TAS displayed as a (a) false colour heat map and (b) lineouts at selected pump-probe time delays for **1** photoexcited at 306 nm in ethanol. In (a) time delay is plotted linearly until 2 ps and then as a logarithmic scale between 2 and 3000 ps. (c) Transients at selected wavelengths for **1** photoexcited at 306 nm in ethanol. The open circles are the raw data, and the solid lines are the fit.

Table S3. Extracted lifetimes from the global sequential fit of **1** in aqueous solution and in ethanol. The associated errors quoted by our fitting software were smaller than our instrument response and so here the errors are given as half of our instrument response, with the exception of τ_2 in ethanol.

	τ_1 (fs)	τ_2 (ps)	τ_3 (ns)
1 (aqueous)	110 ± 40	1.21 ± 0.04	> 3
1 (ethanol)	440 ± 40	18.01 ± 0.27	> 3

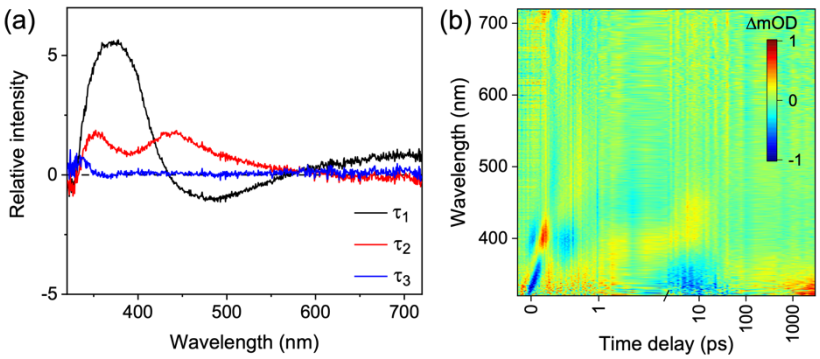

Figure S18. (a) Evolution associated difference spectra for **1** photoexcited at 306 nm in ethanol. (b) False colour heat map of the fitting residual of **1** photoexcited at 306 nm in ethanol.

Triplet vertical excitation energies

Table S4. Calculated triplet vertical excitation energies for the optimised S_0 geometries of **1**-**4** (lowest energy conformer) in implicitly modelled water at the RI-CC2/def2-TZVP level.

Molecule (conformer)	State	Energy (eV)	Energy (nm)	Character
1 (a)	T_1	3.50	354	ππ*
	T_2	3.98	312	nπ*
	T_3	4.28	290	ππ*
2 (b)	T_1	3.40	365	ππ*
	T_2	3.96	313	nπ*
	T_3	4.26	291	ππ*
3 (b)	T_1	3.31	375	ππ*
	T_2	3.97	313	nπ*
	T_3	4.26	291	ππ*
4 (b)	T_1	2.94	422	ππ*
	T_2	4.21	294	nπ*
	T_3	4.60	270	ππ*

Fluorescence spectra

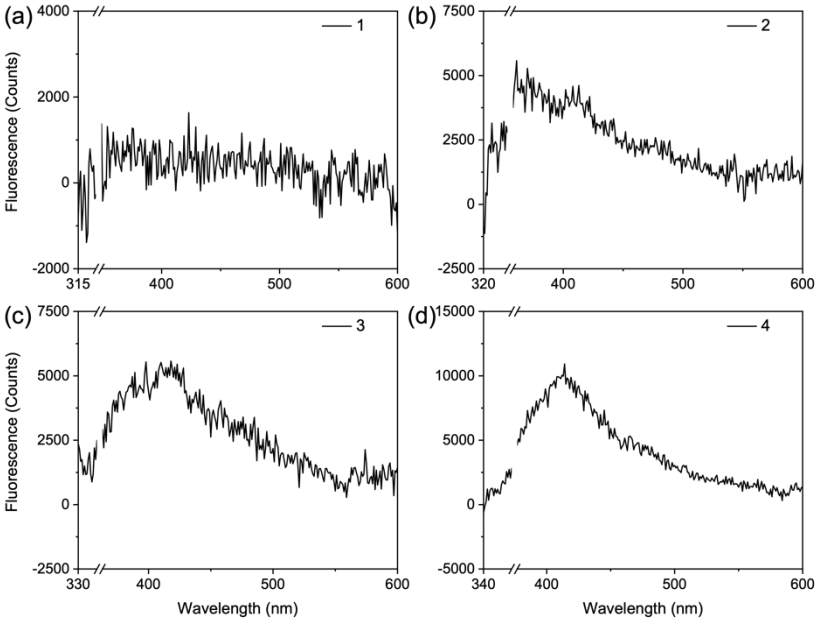

Figure S19. Fluorescence spectra of ~15 μM aqueous solutions of (a) **1** photoexcited at 306 nm, (b) **2** photoexcited at 314 nm, (c) **3** photoexcited at 318 nm and (d) **4** photoexcited at 331 nm.

Conformer vertical excitation and relative energy discussion

Figure S20 below is a schematic representation similar to **Figure S7** but with additional information. **Figure S20**a displays a skeletal structure of **1** with the C–C–N–C dihedral angle highlighted in pink. The relative energies of each conformer, their optimised geometries, their C–C–N–C angle, and predicted peak absorptions are presented in **Figure S20**b. A discussion of the relative energy of the conformers and their geometries has been discussed earlier so will not be revisited here, instead focus will be on the predicted peak absorptions. These have been determined by summing Gaussians of the first five singlet vertical excitation energies with a fixed width of 0.2 eV for each Gaussian. In the case of **2**-**4**, there is a slight red-shifted absorption for the higher energy conformer. For **1** this is not the case, however, the absorption of the higher energy conformer is very close to the lower energy conformer and has a higher oscillator strength (values reported in **Table S1**). These results would provide a plausible explanation for the excited state absorptions at 3 ns observed in the TEAS if rotation around the C-3–N bond was the photoprotection mechanism followed. To probe this further, the C–C–N–C dihedral angle of **1** was rotated to +90°/-90°, fixed and then optimised to give an approximate transition state geometry. The lower energy of the two being -90° was then used to perform a transition state optimisation with no dihedral angle constraints which converged to a geometry which had a C–C–N–C dihedral angle of -112° and a relative energy of ~0.5 eV above conformer **a** (the lowest energy conformer). This is a similar energy barrier to what Losantos *et al.*[6] found for the cyclohexenimine chromophore (note that this is not the same chromophore as within this work) disubstituted with phenyl rings and the authors suggested that the photoisomer could thermally convert back to the original isomer at room temperature likely without any accumulation of the photoisomer. Note that our calculations have not investigated the photoprotective mechanism in any detail, this being through excited state relaxation calculations or conical intersection searches as we feel this to be beyond the scope of the present study. As a result, we cannot draw any clear conclusions about the origin of the excited state absorption (blue edge of the probe window) at 3 ns. Instead, we can suggest that isomer formation is plausible and so is minor trapped population in the S_1 excited state following a planar to non-planar ring buckling mechanism based on the detailed computational studies performed by Losantos *et al.*[6,7]

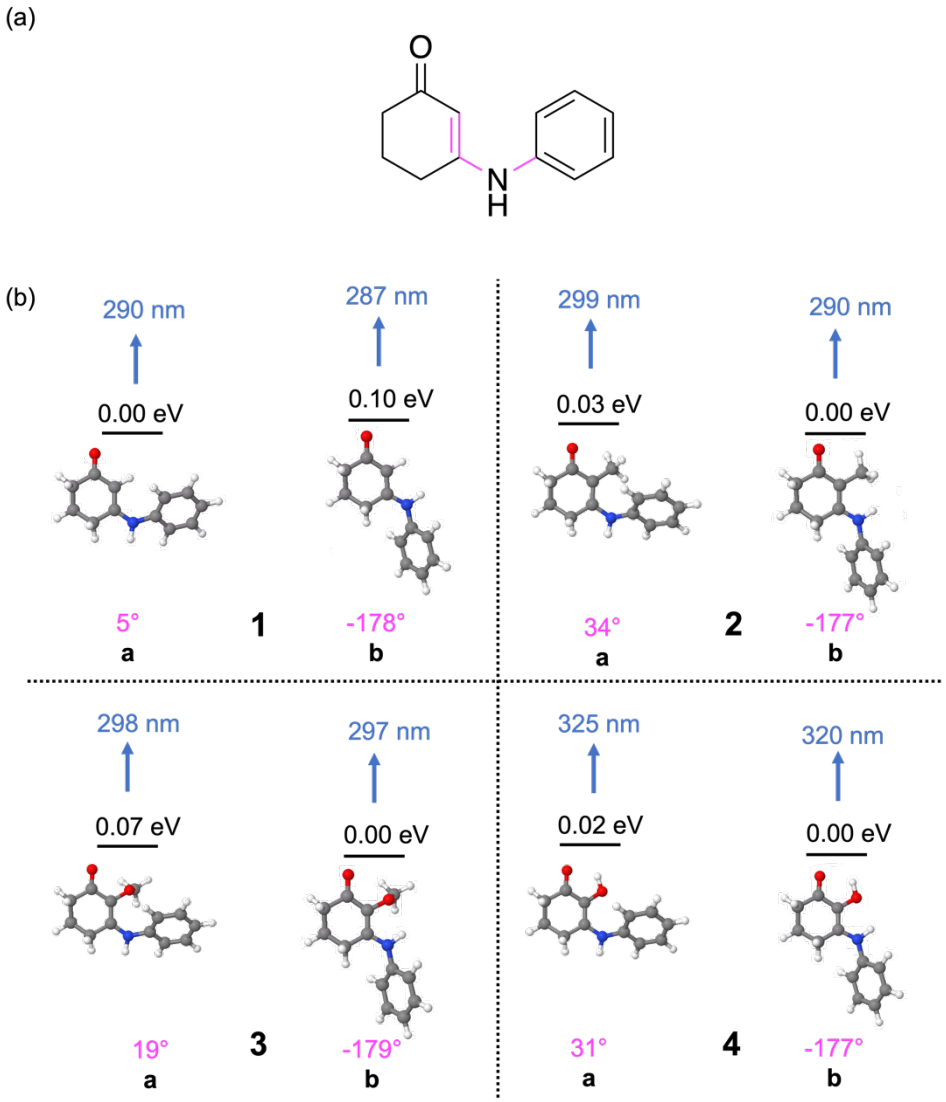

Figure S20. (a) Structure of **1** with the C–C–N–C dihedral angle highlighted in pink. (b) Schematic representation of the relative energies of the conformers of **1**-**4** with respect to their lowest energy conformer along with their optimised geometries and the C–C–N–C dihedral angles of each conformer reported in pink. Also reported is the predicted peak absorption determined by the sum of Gaussians with a fixed width of 0.2 eV for the first five singlet vertical excitation energies. Note that (b) is not drawn to scale.

Long-term irradiation detailed discussion

As can be observed in **Figure S21**, the UV-visible spectra following irradiation with a solar simulator of molecules **1**-**3** only mildly change. In fact, over the UVB and UVA regions, <6% degradation was observed which we believe could be due to the trapped S_1 population beyond 3 ns or the broader irradiation spectrum output by the solar simulator possibly enabling absorption of higher energy photons and alternative reaction coordinates to become available; see **Figure S22** for the solar spectrum. Note that when considering a molecule as a potential UV filter, we tend to quote any degradation less that 20% as a photostable molecule loosely based on the work by Gonzalez *et al.*[8] and Hojerová *et al.*[9] Further to this, no new absorptions were observed in the ~350-400 nm region, which would correspond to the long-lived species in the TAS. This confirms that the long-lived feature in the TAS at 3 ns is not due to a stable photoproduct, *i.e.* the higher energy conformer if formed thermally returns to equilibrium beyond 3 ns as described earlier.

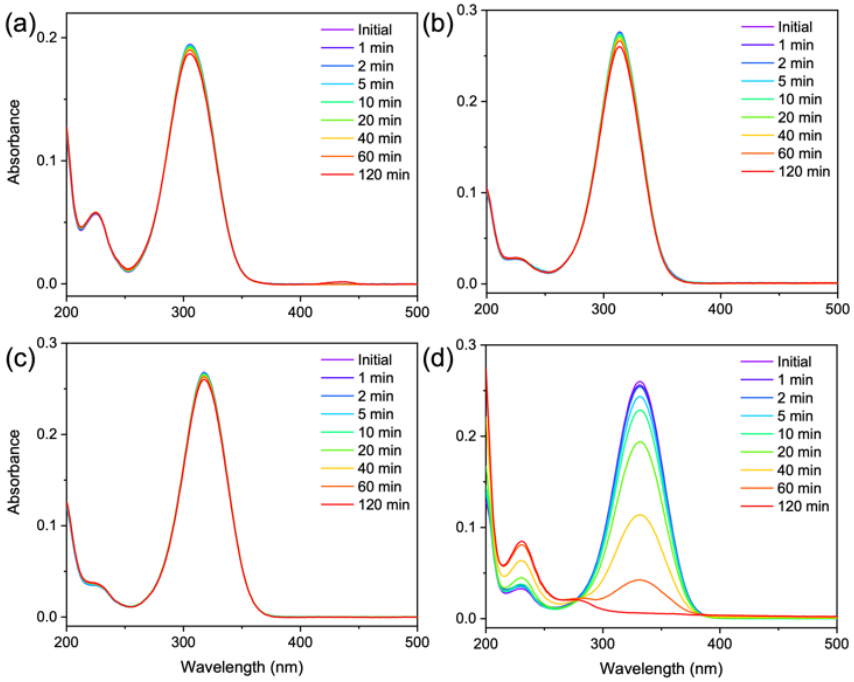

Figure S21. UV-visible spectra over 120 minutes of irradiation with a solar simulator for ~10 µM aqueous solutions of (a) **1**, (b) **2**, (c) **3** and (d) **4**.

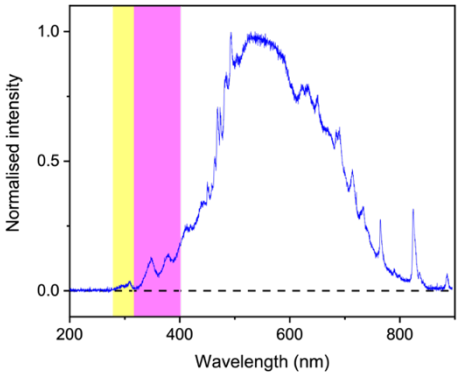

Figure S22. The spectrum output by the solar simulator used for the irradiation experiment in this work. Highlighted in yellow is the UVB region (280-315 nm) and highlighted in pink is the UVA region (315-400 nm).

In comparison, for **4**, the main peak at 331 nm has almost completely disappeared after 120 minutes of irradiation with a solar simulator. In addition to this, the smaller peak at ~230 nm has increased in intensity and a second lower intensity peak at 280 nm is revealed. These peaks being at a lower wavelength (higher energy) implies that loss of conjugation in the molecule is occurring. To probe this further, a ^{1}H NMR spectrum pre- and post-irradiation was acquired and as expected new peaks were present in the post-irradiated spectrum; see **Figure S23**. One theory is that hydrolysis back to the starting materials occurs. However, the new peaks do not correspond to dihydropyrogallol and aniline (NMRs not shown). Therefore, we can only suggest that **4** likely hydrolyses to products which suggest cleavage of the C-3–N bond but the products themselves have not been identified. Why this is only observed for **4** and not the other studied molecules is also unknown but the presence of the intramolecular hydrogen bond may play a role.

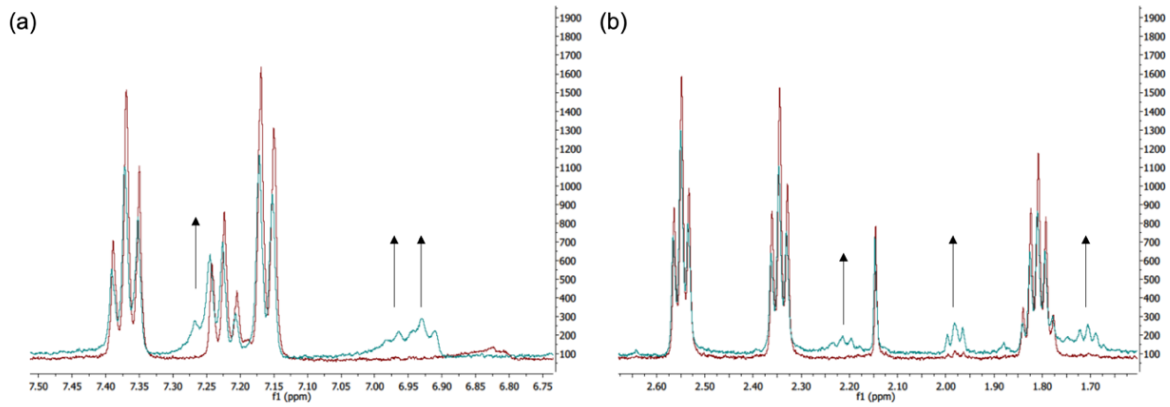

Figure S23. ^{1}H NMR spectra of **4** pre- (red trace) and post- (green trace) solar simulator irradiation around (a) 7 ppm and (b) 2 ppm. Black arrows indicate where new peaks emerge in the post-irradiated spectrum.

Interestingly, when a solution of **4** is left in the dark for 120 minutes, we observed a 20% degradation at the peak suggesting that this hydrolysis occurs in the dark and at room temperature implying that an aqueous solution of **4** is not chemically stable; see **Figure S24**. Our solar simulator irradiation showed higher levels of degradation than the control and whilst we expose the solution to light, the box containing this experiment where the cuvette is placed reaches elevated temperatures of ~35°C, a consequence of our experimental setup. To explore whether heat or light accelerates the hydrolysis, we conducted two separate experiments. Firstly, we heated a solution to 50°C for 60 minutes and saw elevated levels of degradation compared to the room temperature, dark control. Therefore, heat impacts the rate of degradation. The second experiment was monochromatic irradiation at 331 nm which was conducted close to room temperature conditions (tests revealed that the temperature in the irradiation chamber increased by ~2°C). Note that again increased levels of degradation was observed suggesting that light also accelerates the process. Both of these results are presented in **Figure S25**.

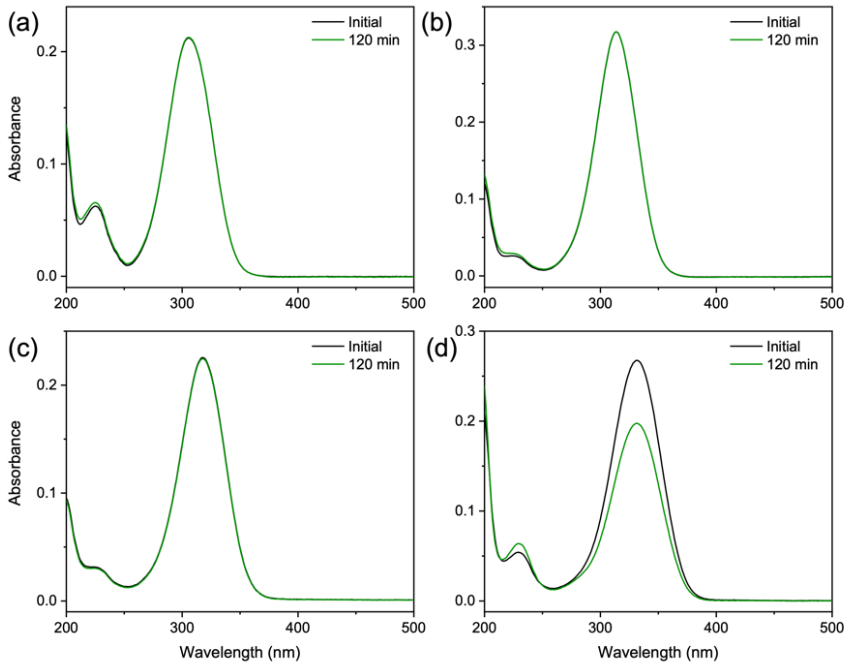

Figure S24. UV-visible spectra before and after 120 minutes of being left in the dark for ~10 µM aqueous solutions of (a) **1**, (b) **2**, (c) **3** and (d) **4**.

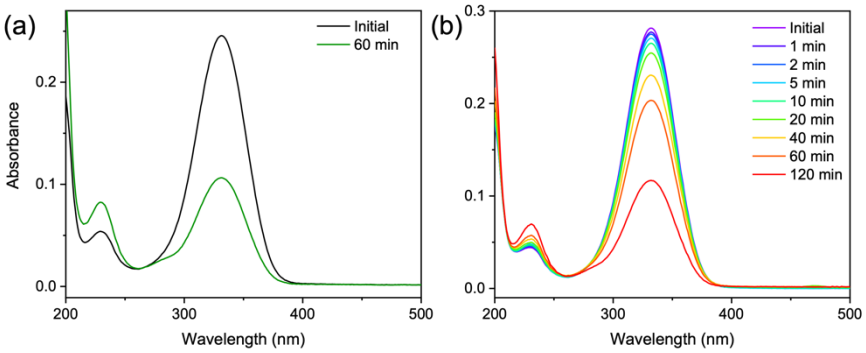

Figure S25. (a) UV-visible spectra before and after 60 minutes of heating at 50°C of ~10 µM aqueous solution of **4**. (b) UV-visible spectra over 120 minutes of continuous irradiation at 331 nm of ~10 µM aqueous solution of **4**.

With all of this in mind, we can be confident that this hydrolysis occurs in the electronic ground state, however, we cannot be so certain whether the hydrolysis also occurs in the electronic excited state. This is because the products which absorb at ~230 nm and ~280 nm are outside the probe window in our TEAS so we cannot learn of the lifetimes associated with their production. Furthermore, it is possible that the hydrolysis occurs as a result of degradation of the long-lived product beyond 3 ns. The most probable cause of accelerated degradation with heat compared to a dark control is that the electronic ground state reaction coordinate for the hydrolysis has a barrier that is more easily overcome with the additional heat energy. With respect to the accelerated light degradation, a possibility is that upon photoexcitation, **4** undergoes a geometry rearrangement to reach the S_1/S_0 conical intersection. Once population is on the vibrationally hot electronic ground state, the reaction coordinate forks and the population can either reform the original electronic ground state which is evidenced by the GSB recovery, or it can follow the hydrolysis reaction coordinate.
In contrast, this degradation is not observed for the other substituents. As suggested in the main manuscript, one hypothesis is that the intramolecular hydrogen bond in **4** destabilises the molecule making it more prone to hydrolysis. Regardless, as a design guideline for the future, it would be wise to avoid hydroxy substituents in these mycosporine-inspired molecules. In fact, one step in the natural synthesis of mycosporine-glycine converts dimethyl 4-deoxygadusol to 4-deoxygadusol, see **Scheme S1**, which involves the conversion of the hydroxy group at the C-2 position to a methoxy group.[10] We tentatively suggest that the conversion of the hydroxyl group to a methoxy group by nature is an evolutionary strategy to avoid potential instability. Further to this, this result aligns with reports that normycosporines are unstable molecules and prone to hydrolysis.[11,12]

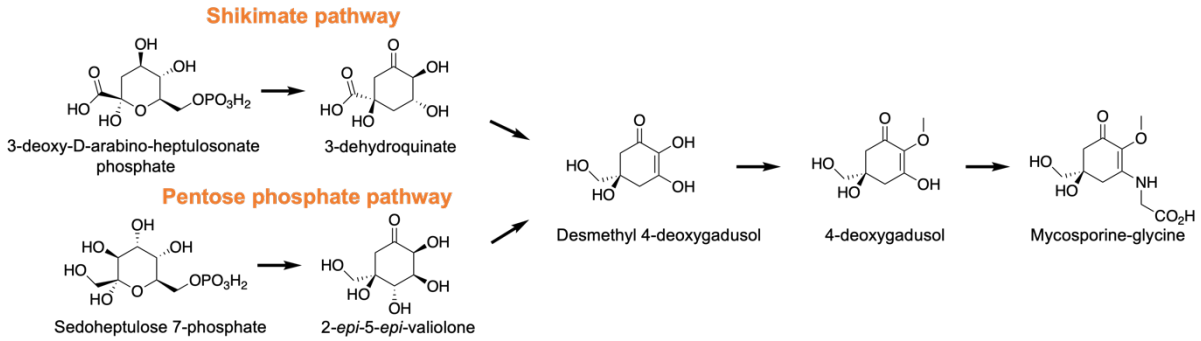

Scheme S1. Biosynthesis of mycosporine-glycine via the shikimate pathway and the pentose phosphate pathway.

References

1. T. Wang, G. Chen, Y.-J. Lu, Q. Chen, Y. Huo and X. Li, *Adv. Synth. Catal.*, 2019, **361**, 3886-3892.
2. J.-C. Gramain, H.-P. Husson and Y. Troin, *Tetrahedron Lett.*, 1985, **26**, 2323-2326.
3. W. Mayer, R. Bachmann and F. Kraus, *Chem. Ber.*, 1955, **88**, 316-329.
4. B. Pecherer, L. M. Jampolsky and H. M. Wuest, *J. Am. Chem. Soc.*, 1948, **70**, 2587-2589.
5. A. L. Whittock, N. Auckloo, A. M. Cowden, M. A. P. Turner, J. M. Woolley, M. Wills, C. Corre and V. G. Stavros, *J. Phys. Chem. Lett.*, 2021, **12**, 3641-3646.
6. R. Losantos, I. Lamas, R. Montero, A. Longarte and D. Sampedro, *Phys. Chem. Chem. Phys.*, 2019, **21**, 11376-11384.
7. R. Losantos, I. Funes-Ardoiz, J. Aguilera, E. Herrera-Ceballos, C. García-Iriepa, P. J. Campos and D. Sampedro, *Angew. Chem. Int. Ed.*, 2017, **56**, 2632-2635.
8. H. Gonzalez, N. Tarras-Wahlberg, B. Strömdahl, A. Juzeniene, J. Moan, O. Larkö, A. Rosén and A.-M. Wennberg, *BMC Dermatol.*, 2007, **7**, 1-9.
9. J. Hojerová, A. Medovcíková and M. Mikula, *Int. J. Pharm.*, 2011, **408**, 27-38.
10. M. A. Pope, E. Spence, V. Seralvo, R. Gacesa, S. Heidelberger, A. J. Weston, W. C. Dunlap, J. M. Shick and P. F. Long, *ChemBioChem*, 2015, **16**, 320-327.
11. J. Bernillon, M.-L. Bouillant, J.-L. Pittet, J. Favre-Bonvin and N. Arpin, *Phytochemistry*, 1984, **23**, 1083-1087.
12. M.-C. Lunel, N. Arpin and J. Favre-Bonvin, *Tetrahedron Lett.*, 1980, **21**, 4715-4716.